HEFAT2012
9th International Conference on Heat Transfer, Fluid Mechanics and Thermodynamics
16 – 18 July 2012
Malta

NON-ADIABATIC TURBULENT ULTRA RICH COMBUSTION OF NATURAL GAS

Kok J.B.W.*, Albrecht B.A. and Woolderink M.H.F.
*Author for correspondence
Department of Engineering Technology, Laboratory of Thermal Engineering,
University of Twente,
P.O. Box 216, Enschede
The Netherlands,
E-mail: j.b.w.kok@utwente.nl

ABSTRACT

In rich combustion, the natural gas is partially oxidized to produce syngas, a mixture which consists mainly of hydrogen and carbon monoxide. The goal of the work is to develop a computational model to predict the syngas composition, temperature and soot content. The method of reaction progress variables is applied to turbulent rich combustion modeling. The model handles both the gaseous and the solid phase transport. The gas phase model predicts the gaseous chemical species and temperature. The soot model quantifies the soot formation in the turbulent rich flame. The link between the two parts is the concentration of acetylene, which is considered to be the dominant soot precursor. The model is implemented in the CFX flow solver. The model predictions are compared with data from experiments on ultra rich combustion of natural gas by means of air enriched to 40% oxygen concentration at up to 3 bar and 300 kW. Good comparison was found between measurements and model predictions on carbon monoxide, hydrogen and the soot precursor acetylene. It can be concluded that the model provides reliable information on product gas concentrations as a result of ultra rich combustion of natural gas. The predicted soot concentrations were found to compare well to measurements in a rich flame as reported in the literature.

INTRODUCTION

Ultra rich combustion (gasification) of hydrocarbons is a process applied to produce synthesis gas (or syngas). This gas is composed primarily of hydrogen and carbon monoxide. Syngas represents the intermediary step from hydrocarbons to bulk chemicals (for example acetic acid, methanol, DME, oxo-alcohols, isocyanates, ammonia) and synthetic fuels (synthetic Diesel). The ultra rich combustion of methane can be described by the following global reaction:

$$CH_4 + 0.5O_2 = CO + 2H_2, \quad \Delta h = -36 \text{ kJ/mol} \qquad (1)$$

In eq. (1), the negative value of the heat of reaction Δh indicates that the rich combustion process is exothermic when viewed from reactants to products.. In industrial applications of this process, temperatures range between 1400 and 1800 K and pressures are up to 150 bar, see [1], [2]. To analyze the performance of the reactor with a view to bulk chemicals production, the composition of the syngas can be estimated at equilibrium. This estimate is however very inaccurate, as in practical reactor designs the syngas is produced in conditions far from chemical equilibrium. For this reason, the chemical away-from-equilibrium performance of the ultra rich combustion reactor, taking chemical kinetic effects into account, is important. The reactor design and the operating conditions have to ensure a high conversion of natural gas to products (hydrogen and carbon monoxide). The syngas soot content is of concern, in view of the syngas fouling the reactor and downstream system. For these reasons the rich combustion process inside the reactor is investigated in the present paper, taking into account chemical kinetics and turbulent transport. For the natural gas (NG) the composition is taken as 85 % vol. CH_4 and 15 % vol. N_2. This composition was chosen to give the lower heating value of the Dutch natural gas produced by the Groningen reservoir [3]. The oxidizer is oxygen enriched air (hereafter abbreviated as NITROX), composed of 40 % vol. O_2 and 60 vol. %. N_2.

In a previous paper [4], the reactor was simulated in a freely propagating flame and in a perfectly stirred reactor. These simplified models provided information on the structure of rich flames as those obtained by partial oxidation. They also showed the effect of different parameters (pressure, residence time, equivalence ratio, type of mixture) on the syngas composition. This data is used to model the partial oxidation reactor for the actual operating conditions. The operating conditions for the large scale application of the partial oxidation process are characterized by turbulent flow and a high fuel to oxidizer ratio. In this paper the rich combustion process is investigated in the situation that natural gas and oxidizer are perfectly premixed.

That way the research can be focused on the chemical kinetics, heat loss and the interaction with turbulence. The gaseous chemistry is described by a detailed reaction mechanism. The soot formation is described by the processes of nucleation, surface growth, agglomeration and oxidation. The numerical model predicts the flow field, gaseous species (especially H_2, CO, C_2H_2), temperature and soot (mass fraction and number of particles). The model is presented in the following.

NOMENCLATURE

Latin symbols

C	[-]	model constant
D	[m^2 s^{-1}]	molecular diffusion coefficient
d_p	[m]	mean soot particle diameter
d_1	[m]	reactor diameter
d_2	[m]	burner inner diameter
d_3	[m]	burner tip diameter
f_S	[-]	soot volume fraction
h	[kJ/kg]	specific gas enthalpy
k	[m2/s2]	turbulent kinetic energy
N	[1/m3]	particle number density
P	[-]	probability density function
P_j	[N/m2]	partial pressure of species j
i	[-]	heat loss variable
r	[-]	hydrogen reaction progress variable
T	[K]	temperature
S	[kg m^{-3} s^{-1}]	chemical source term
S	[m^{-3} s^{-1}]	source term soot particles
U	[m/s]	gas velocity
Y_j	[-]	mass fraction of species j
Y_S	[kg soot kg^{-1}]	soot mass fraction
Z	[-]	denominator of r definition relation

Greek symbols.

ρ	[kg/m3]	specific gas density
Γ	[m2/s]	diffusion coefficient
μ	[kgm/s2]	dynamic viscosity
σ	[-]	Prandtl number
σ	[kg s^{-3} K^{-4}]	radiation constant
ε	[m2/s3]	rate of dissipation turbulent kinetic energy

TURBULENT RICH COMBUSTION MODEL

The computational model for the turbulent rich combustion process is structured in three interlinked parts. Part one is the gas phase model, that predicts the gaseous chemical species concentrations. The second part is the luminous radiation model, that predicts the local gas temperature consistent with the local species concentrations and soot related radiation heat loss. Part three is comprised by the soot model, that quantifies the soot formation in the turbulent rich flame. The two parts are linked by the concentration of acetylene, which is the soot precursor, and the heat loss that results from luminous heat radiation of the soot particles and gas-solid heat exchange. The gas phase model is described in this section; the soot model is described in the next.

In the gas phase model, the basis for the detailed chemistry is given by the GRI-Mech 3.0 chemical reaction mechanism for Natural Gas[5]. For a combustion simulation with the GRI-Mech 3.0 mechanism, 53 chemical species transport equations and the enthalpy equation must be solved. In laminar flows it is possible to solve this system. Under turbulent conditions to solve the flow field and the transport equations for such a large number of independent variables is computationally prohibitive. That is why the number of independent variables which describe the turbulence-chemistry interactions has to be minimized. In the present model, the reduction of the variables set is achieved by mapping of the gaseous chemical system on two combustion scalars. This is described in the sections below.

Enthalpy, temperature and radiative heat loss.

In sooting flames, like the ultra rich flame, soot is the primary source of heat loss by radiation. To account for this effect, an enthalpy variable was introduced, denoted i. This is defined as the enthalpy loss normalized through the adiabatic enthalpy value and takes the value 0 for the adiabatic case and positive values for non-adiabatic situations. The definition relation is

$$i = \left| \frac{h_{ad} - h}{h_{ad}} \right|, \qquad (2)$$

where h is the local enthalpy value and h_{ad} is the adiabatic enthalpy, equal to the enthalpy of the initial mixture. Please note that the enthalpy (including enthalpy of formation) is always negative and smaller than or equal to the adiabatic value. The Favre-averaged steady state turbulent transport equation for the enthalpy variable reads

$$\nabla\left(\bar{\rho}\tilde{\mathbf{u}}\tilde{i}\right) - \nabla\left(\Gamma_{eff}\nabla\tilde{i}\right) = \bar{S}_i, \qquad (3)$$

where ρ is the mixture density, **u** is the velocity vector, $\Gamma_{eff,i}$ is the effective diffusion coefficient of variable i and S_i is the heat loss due to the radiation of soot. The effective diffusion coefficient is defined as

$$\Gamma_{eff,i} = \rho D_i + \frac{\mu_T}{\sigma_T}, \qquad (4)$$

where D_i is the molecular diffusion coefficient of variable i, μ_T is the turbulent viscosity and σ_T is the turbulent Prandtl number. The turbulent viscosity is calculated on basis of the expression given in eq. 5, with the model constant Cμ=0.09. The effect of turbulence on scalar mixing is given by the values of k and ε, as calculated by the transport equations for these variables, see [6],[7].

$$\mu_T = C_\mu \rho \frac{k^2}{\varepsilon} \qquad (5)$$

The heat loss due to the radiation of soot, S_i, is given by

$$S_i = -\frac{4C_0\sigma_0 f_S\left(T^5 - T_{wall}^5\right)}{h_{ad}}. \qquad (6)$$

In Eq. (6), $C_0 = 1.307\cdot10^3$ m^{-1} K^{-1} is a soot radiation constant [8], $\sigma_0 = 5.6704 \times 10^{-08}$ kg s^{-3} K^{-4} is the Stefan-Boltzmann constant, f_S is the soot volume fraction, T is the soot temperature and T_{wall} is the reactor wall temperature. The heat loss due to radiation of soot from Eq. (6) is based on the expressions given in [8,9,10]. The averaged source term in Eq. (6), $\overline{S}_i$, is calculated as described in the next section. The radiation of soot is assumed to be dominant over gaseous radiation and the latter is therefore not taken into account.

Reaction progress variable modeling.

The local chemical species concentrations are to be predicted by a reaction progress variable, that increases monotonically with the advance of the gaseous chemical reactions. In the Turbulent Flame Speed Closure model, often applied for adiabatic premixed turbulent flames, for this variable the flame temperature is chosen. In the rich combustion process, with endothermal reforming reactions and soot formation at significant heat loss, there is not a unique relation any more between temperature and progress of chemical reactions. For that reason, here a characteristic monotonically decreasing fuel species is chosen for the RPV construction, namely H_2. This variable is denoted by r and represents the normalized mass fraction of H_2. It takes values between 0 in the initial mixture and 1 in the burnt gas. The definition relation is

$$r = \frac{Y_{H_2} - Y_{H_2}^{in}}{Y_{H_2}^{eq} - Y_{H_2}^{in}}, \qquad (7)$$

where $Y_{H_2}^{in}$ and $Y_{H_2}^{eq}$ are the mass fractions of H_2 at initial conditions and at equilibrium conditions, respectively. By introducing a function Z, the denominator in relation (7) is expressed as

$$Z(i) = Y_{H_2}^{eq} - Y_{H_2}^{in}. \qquad (8)$$

In non-adiabatic combustion, $Y_{H_2}^{eq}$ depends on the heat loss and thus on the enthalpy variable i. It follows that Z is also a function of i. Furthermore, it is assumed that Y_{H_2} and $Y_{H_2}^{eq}$ have a similar dependence on i. As a result, the hydrogen variable r and the enthalpy variable i are considered statistically independent. A similar assumption was made in [11]. The Favre-averaged steady state turbulent transport equation for r reads:

$$\nabla\left(\bar{\rho}\tilde{u}\tilde{r}\right) - \nabla\left(\Gamma_{eff,r}\nabla\tilde{r}\right) = \overline{S}_r - \overline{\frac{1}{Z}\frac{\partial Z}{\partial i}}\tilde{r}\overline{S}_i, \qquad (9)$$

where $\Gamma_{eff,r}$ is the effective diffusion coefficient of variable r, which has an expression similar to eq. (4) and $\overline{S}_r$ is the mean chemical source term of the variable r. The averaged source terms which appear in Eq. (9), $\overline{S}_r$ and $\overline{S}_i$, are calculated by Probability Density Function (PDF) averaging of the source terms S_r and S_i, respectively, with the joint PDF of the variables r and i. The expression of $\overline{S}_r$ is then:

$$\overline{S}_r = \int_0^1\int_0^1 S_r P(r,i)\,dr\,di = \int_0^1\int_0^1 S_r P(r)P(i)\,dr\,di, \qquad (10)$$

where P(r,i) is the joint PDF of variables r and i, P(r) is the PDF of variable r and P(i) is the PDF of variable i. A similar relation defines the averaged source term of variable i, $\overline{S}_i$. In Eq. (10), due to the assumed statistical independence of variables r and i, the joint PDF equals the product of the independent PDFs. Following the definition (2), the enthalpy variable i can also take values greater than 1. However, usually values of heat loss by soot radiation result in values of the variable i between 0 and 1. Therefore, the range of variation for the variable i in Eq. (10) was taken from 0 to 1. For the individual PDFs of r and i, the assumed shape function approach was used. The assumed shape of such a PDF can be a delta or a beta function. In the simulations to be presented later in this paper, the delta shaped functions were employed. This means that the effect of the turbulent fluctuations on the progress of chemical reactions and the heat loss has been neglected. This choice is justified by the fact that the uncertainties related to the description of the gas phase chemistry and the soot formation processes in the premixed rich flames were considered more important than those introduced by neglecting the turbulent fluctuations.

Thermo-Chemical Database.

The source term of i, given by relation (6), is a function of soot volume fraction and temperature. As to be described in a later section, soot mass fraction is mainly a function of acetylene concentration and temperature (it also depends on the mass fractions of hydrogen and hydrogen atoms through the surface growth mechanism). The source term of r in Eq. (10) is a function of the chemical species mass fractions and temperature. In the same equation, the factor which contains the function Z (called hereafter the Z factor) is a function of the enthalpy variable i. The reduction of the number of scalars describing the combustion is achieved by pre-calculating the species mass fractions and temperature as functions of r and i. In order to speed up the flame calculations, the density, the source term of r and the Z factor are also calculated in a pre-processing step as functions of the combustion scalars r and i. All these quantities are stored in a thermo-chemical database as

functions of discrete values of r and i. This database is a look-up table which is accessed during the flame calculation by the flow solver to retrieve the source term of r, the density, the temperature, the acetylene mass fraction, the mass fractions of hydrogen and hydrogen atoms and the Z factor for the integration of the transport equations of r, i, Y_S and N_S. The database is also used to get the final fields of species mass fractions and temperature based on the computed solution for r and i.

In principle, a thermo-chemical database which is used in a RPV combustion model, as that described in this paper, is created by solving a system of (N + 1) nonlinear equations, N for chemical species and one for the enthalpy (N stands for the number of species) as described in [12,23]. The independent variables are the reaction progress variable r and the enthalpy variable i and the unknowns are the species mass fractions and the temperature. Due to the convergence difficulties associated with solving highly nonlinear systems of equations and the complex nature of the chemical system under investigation (ultra rich conditions), an alternative way for calculating the database was used. Because of the intensely turbulent nature of the present combustion process, the combustion was considered to take place within the distributed reaction zone regime. The microstructure of the distributed reaction zone was modeled as a spectrum of perfectly stirred reactors over a range of residence times and heat losses. A similar approach was reported in [13] with good results. The database was generated by using the PSR code of the CHEMKIN-II chemical kinetics package [14]. Each set of values of the residence time and the heat loss leads to a composition, a temperature and the corresponding enthalpy. Based on the composition, the reaction progress variable r can be calculated. Given the enthalpy, the enthalpy variable i can be derived. This way, every pair of values of the residence time and the heat loss results in a pair of combustion scalars values (r, i) which corresponds to a composition and a temperature of the mixture. The composition and the temperature of the mixture at equilibrium (r = 1) was evaluated with the EQUIL code. The minimum calculated value of r for which the PSR code gave a solution was around 0.2. For residence times corresponding to r below this value, the mixture did not ignite because of the low temperature. To evaluate the composition of the mixture for the values of r between 0 and 0.2, an ignition model was built. This was based on solutions of freely propagating flames simulated with the PREMIX code, using a similar procedure with that described for the PSR calculations. EQUIL and PREMIX are both codes of CHEMKIN-II software. In order to show the properties of such a thermo-chemical database, plots of a database to be used for numerical simulations are presented in the following. The specifications of the mixture for which the database was calculated are given in Table 1.

Table 1. Specifications of the NG/NITROX mixture for which the database was calculated.

Natural Gas (NG)	CH_4 : 85 %, N_2 15 %
Oxidizer (NITROX)	O_2 :40 % N_2 :60 %
NG/NITROX mixture parameters	Equivalence ratio 3.1
	Initial temperature: 673 K
	Pressure: 6 bar

Figures 1 and 2 present the temperature and the acetylene mass fraction, respectively, as functions of the reaction progress variable r, for different values of the enthalpy variable i. It can be seen that the temperature has a peak for r close to 0.3 and then decreases to the equilibrium value at r equals 1. This behavior of temperature in rich chemical systems is in contrast with lean or stoichiometric mixtures for which the maximum temperature is attained at equilibrium. The explanation is that a rich combustion process takes place in two global steps. In the first step a part of the fuel and all the oxidizer are converted through exothermic reactions to water and carbon dioxide. This leads to the initial increase of the temperature. In the second step the rest of the fuel is reformed by water and carbon dioxide to give hydrogen and carbon monoxide. This second step is endothermic and first counterbalances the temperature increase until it reaches its maximum and then provokes the observed decrease of the temperature towards the equilibrium value. The variation of the temperature with i is as expected: temperature decreases when i (heat loss) increases.

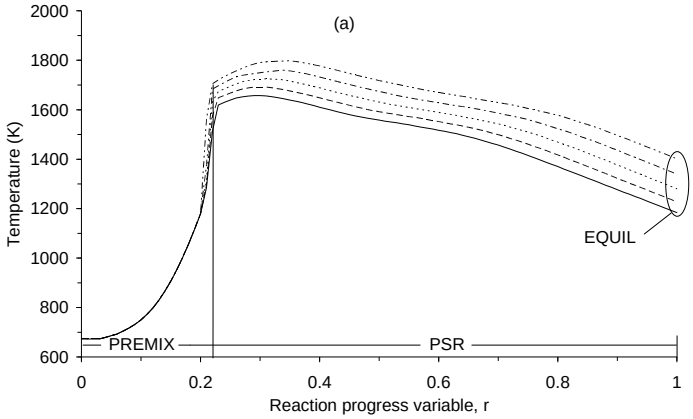

Figure 1 Temperature as a function of reaction progress r. The value of i is 0 at the top curve and increases in lower curves.

In figure 2, it appears that the acetylene follows the path of an intermediate, with zero values of the mass fraction in initial mixture (r = 0) and at equilibrium (r = 1) and a peak in between. The variation of the acetylene mass fraction with i follows that of the temperature: it decreases with increasing i. Another species dependent on temperature is the hydrogen atom.

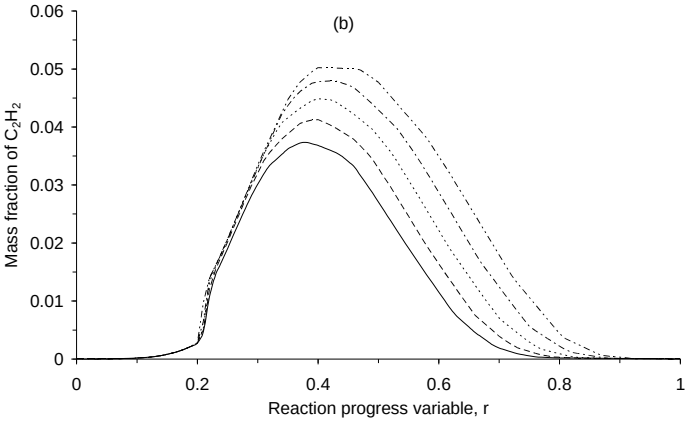

Fig. 2 Acetylene mass fraction as a function of reaction progress r. The value of i is 0 at the top curve and increases in lower curves.

Figure.3 shows the hydrogen atom mass fraction as a function of r and i. The hydrogen atoms have an intermediate species behavior in r direction and its mass fraction decreases with the increase of the enthalpy variable. The variation of both acetylene and hydrogen atom concentration with temperature is important for the prediction of soot formation to be discussed in the next section. The last picture presented, Figure 4, is the source term of r as function of r and i. The chemical source term is zero in the initial mixture (r = 0) and at equilibrium (r = 1) and it has a maximum value which decreases with increasing the heat loss.

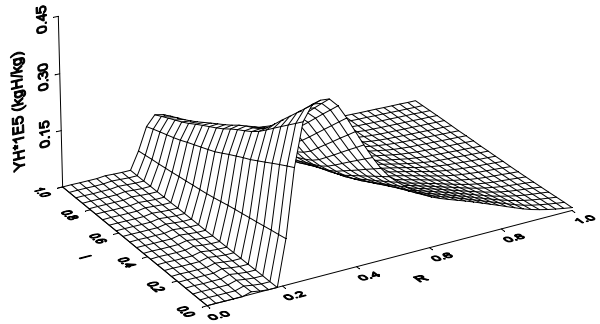

Fig. 3 H mass fraction as a function of reaction progress r and i.

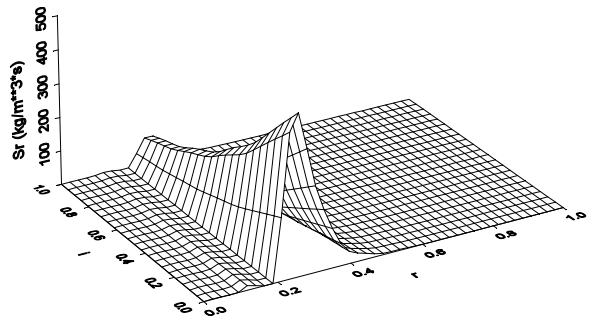

Fig. 4 r source term as a function of reaction progress r and i.

Soot Formation Modeling.

The occurrence of soot in flames, under fuel rich conditions, is well documented [8,9,10,15,16]. Following the mechanism given in [17], soot formation and oxidation is embedded into the detailed description of the gas phase chemistry that provides gaseous species concentrations up to the first aromatic ring, formation and growth of polycyclic aromatic hydrocarbons (PAH) and formation and growth of soot particles by particle inception, surface growth, agglomeration and oxidation. For numerical simulation the mass balances for all the involved chemical species and the enthalpy balance have to be solved. The growth and oxidation of PAH and soot particles are modeled by the H-abstraction-C_2H_2-addition mechanism (HACA). The soot particle phase is treated by means of the balance equation of the moments of the size distribution which leads to a closed system of equations. Detailed modeling results in a large system of equations containing the differential equations for the transport of the mass fractions of the gas phase species, the enthalpy and a limited number of moments of the soot particle size distribution. This large set of differential equations presently can be solved within acceptable computer time for laminar one-dimensional systems only, e.g. premixed flat flames [18]. Due to the turbulent, multidimensional nature of the investigated partial oxidation process, similar to most other practical combustion applications such as gas turbines, gas flares and internal combustion engines, simplified soot models are needed.

Model for Soot based on two turbulent transport equations.

A simplified model of soot formation is used, that distinguishes the processes of nucleation, surface growth, agglomeration and oxidation. The gas phase chemistry is described by the reaction progress variable model, which is based on the detailed reaction mechanism GRI-Mech 3.0. This provides the concentrations of gaseous species throughout the flame, in particular acetylene. The soot nucleation and surface growth are linked to the gas phase chemistry. There are two simplifying assumptions. The first assumption is that acetylene is the indicative species for the locations in the flame where nucleation and soot mass growth occurs. This approach was used by Lindstedt for laminar non-premixed flames [19, 20] and by Brooks and Moss [8] and Kronenburg et al. [9] for turbulent methane diffusion flames. The second assumption is that the consumption of acetylene and other intermediates does not significantly influence their concentrations, and hence does not need to be taken into account.

Nucleation is described in the simplest possible way by a first-order function of acetylene concentration. Surface growth is modeled with the H-abstraction-C_2H_2-addition (HACA) mechanism developed by Frenklach and Wang [21] and used by Xu for rich laminar premixed flames [16, 17]. Particle agglomeration is modeled by the normal square dependence in the free molecular regime, used by many other investigators [8,9,20]. Soot oxidation by O_2 and OH was treated as in

reference [9] while soot oxidation by CO_2, H_2O and H_2 was evaluated using data from reference [22].

Similar to soot modelling in turbulent diffusion flames [8,9], the present model involves the solution of two steady state conservation equations for soot mass fraction Y_S and soot particle number density N_S.

The following expressions for the turbulent transport equations of the soot parameters Y_S and N_S can be formulated:

$$\bar{\rho}\tilde{\mathbf{u}}\nabla\tilde{Y}_S = \nabla\cdot\left(\Gamma_{\text{eff},Y_S}\nabla\tilde{Y}_S\right)+\bar{S}_{Y_S}, \quad (11)$$

$$\bar{\rho}\tilde{\mathbf{u}}\nabla\tilde{N}_S = \nabla\cdot\left(\Gamma_{\text{eff},N_S}\nabla\tilde{N}_S\right)+\bar{S}_{N_S}. \quad (12)$$

In these equations, $\Gamma_{eff,YS}$ and $\Gamma_{eff,NS}$ are the effective diffusion coefficients of Y_S and N_S, respectively. S_{YS} and S_{NS} are the chemical source terms. These source terms are calculated using expressions describing the soot nucleation, surface growth, agglomeration and oxidation, which are presented in reference [2]. The effective diffusion coefficient of Y_S is given by

$$\Gamma_{\text{eff},Y_S} = \rho D_{Y_S} + \frac{\mu_T}{\sigma_T}, \quad (13)$$

where μ_T is the turbulent viscosity and σ_T is the turbulent Prandtl number. The effective diffusion coefficient of N_S has an expression similar to (13).

Also present in Eqs. 11 and 12 are the mean source terms of the soot mass fraction $\bar{S}_{Y_S}$ and the soot particle number density $\bar{S}_{N_S}$. They are found by averaging their laminar expressions given in reference [2], Appendix B, Eqs. B(16) and B(17). Using the simplifying approach of ignoring the effect of turbulent fluctuations on soot parameters, the mean source terms become (see [8]):

$$\bar{S}_{Y_S} = \bar{\alpha}_{Y_S} + \bar{\beta}_{Y_S}\bar{Y}_S^{2/3}\bar{N}_S^{1/3} + \bar{\gamma}_{Y_S}\bar{Y}_S, \quad (14)$$

$$\bar{S}_{N_S} = \bar{\alpha}_{N_S} + \bar{\beta}_{N_S}\bar{Y}_S^{1/6}\bar{N}_S^{11/6}, \quad (15)$$

where $\bar{\alpha}$, $\bar{\beta}$ and $\bar{\gamma}$ are the averaged forms of the functions derived in Appendix B in ref. [2]. They are determined by averaging with the PDFs of the variables r and i, similar with the calculation of the mean source term of r, $\bar{S}_r$, according to

$$\bar{\alpha} = \int_0^1\int_0^1 \alpha P(r,i)\,dr\,di = \int_0^1\int_0^1 \alpha P(r)P(i)\,dr\,di. \quad (16)$$

RESULTS OF SIMULATIONS

The turbulent rich combustion model described above was used to simulate the partial oxidation process of natural gas. Three reactor diameters have been investigated. In Table 1 the gas compositions and operating conditions are given. The NG/NITROX mixture at a pressure of 6 bar and an initial temperature of 673 K was simulated in view of comparison with experiments at the University of Twente. The modeling domain is presented in Figure 5. The NG enters the burner through the inner channel. The NITROX goes into the burner through radial swirl vanes. The NG is mixed with the swirling NITROX flow and the resulted flow enters through an annular channel the partial oxidation reactor. In order to decrease the computational time, the simulations have been carried out in accordance with the following procedure. First a cold flow simulation was performed, to establish the velocity field for the entire geometry presented in Figure 5. Then, a reduced modeling domain was defined, for which the inlet velocity profiles were taken from the previous cold flow simulation. This reduced domain consists of a quarter of a cylinder and has the configuration specified in Figure 5. The grid that meshed the reduced domain was refined in the burner, where the cell size was 1.6 mm. Subsequently, the grid was expanded geometrically with a rate of 1.2 for the full domain simulation and 1.02 for the reduced domain simulations, until a maximum cell size of 4.5 mm was reached. Then, the cell size was kept constant until the end of the domain. The diameter (d_1) and length (L) of the reactor, the inner diameter of the burner (d_2) and the diameter of the burner tip (d_3) are given in Table 2. Also present in Figure 5 are the radial location of the axial plot (y) and the axial locations of the radial plots (x_1, x_2, x_3), which are shown below. These locations are specified in Table 3 as well.

Due to the lack of data from literature and because the soot experiments at the University of Twente are still in an early stage, the predictions of the model could not be validated yet. In order to asses the validity of the soot predictions, results produced by the model are compared with measurements and calculations reported in [16]. It was found that the computed soot mass fraction and particle number density are physically meaningful, but the oxidation rates are over predicting the oxidation of soot by H_2O and CO_2. The explanation is that the reaction rate coefficients used were designed for different C structures and operating conditions [22]. It follows that the oxidation rate parameters have to be adjusted for the present applications by correlating the simulations with experimental data. Since no such data was available, the results presented hereafter were obtained without including the oxidation terms in the soot mass fraction transport equation.

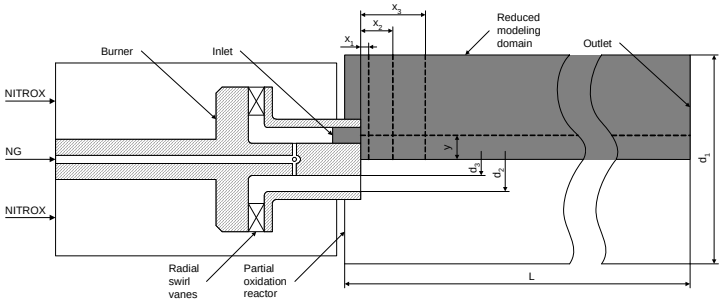

Figure 5 Combustor design and modelling domain for simulations

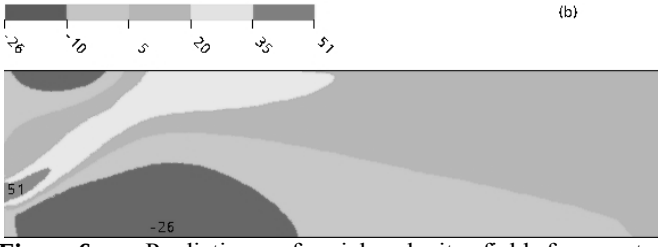

Figure 6 Predictions of axial velocity field for reactor diameter 75 mm. The results have been obtained for a premixed NG/NITROX system with equivalence ratio 3.1, pressure 6 bar and initial temperature 673 K. The numbers which appear in the pictures denote the maximum value (50 or 51 m/s) or the minimum value (-23 or -26 m/s) of the axial velocity. Values in between follow the grey scale shown in the legend.

Reactor Diameter Effect

The effect of the reactor diameter on the conversion efficiency of the partial oxidation process was studied by performing simulations with three diameter values: 50, 75 and 100 mm. For all three cases, the mixture was NG/NITROX, at the conditions specified in Table 1. In Figure 6 the axial velocity fields for the reactor diameter of 75 mm is presented. The burner diameter and the inlet flow conditions are kept constant for all three geometries. They are given in Table 2. Figure 6 shows the presence of a central recirculation zone and a corner recirculation zone. The recirculation zones are created by the expansion of the swirling inlet flow in the reactor.

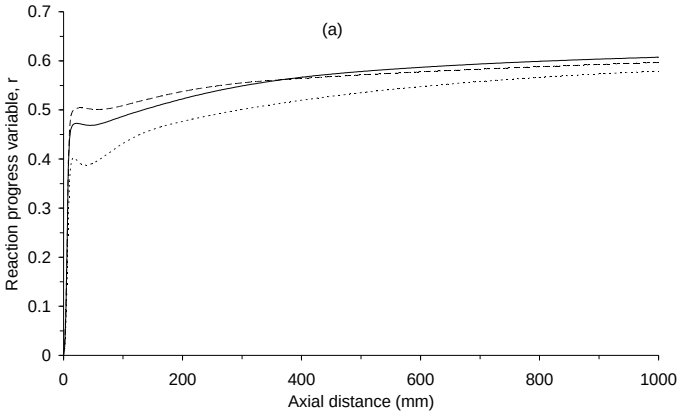

Figure 7 Prediction of axial profiles of the mean of the reaction progress variable r, for reactor diameters: 50 mm (dotted line), 75 mm (solid line) and 100 mm (dashed line). The lines have been drawn through the inlet. Premixed NG/NITROX equivalence ratio 3.1, pressure 6 bar and initial temperature 673 K.

Mixture	NG/NITROX
Reactor diameter, d_1 (mm)	50; 75; 100
Burner inner diameter, d_2 (mm)	25
Burner tip diameter, d_3 (mm)	12.5
Reactor length, L (mm)	1000
Axial velocity (m s^{-1})	50
Reynolds number	50000
Swirl number	0.69

Table 2. reactor dimensions.

Figures 7-10 present the axial profiles of the reaction progress variable r, the soot mass fraction Y_S and the soot particle number density N_S, the enthalpy loss variable i, the temperature, respectively, for the three diameters. The axial plots were made at a radial distance of y = 8.75 mm from the reactor centerline, as shown in Figure 5. In Figure 7, the progress of the chemical reactions is indicated by the evolution of r. The picture shows a very fast increase of the RPV r in the first 20 mm of the reactor length. Thus, r increases from 0 (in the inlet) to 0.41 for the 50 mm diameter, to 0.47 for the 75 mm diameter and to 0.51 for the 100 mm diameter. After this initial zone of fast increase, r continues to rise along the reactor, with higher values for higher reactor diameters. At a distance of 350 mm from the inlet, however, this trend changes and the curves corresponding to 75 and 100 mm reactor diameter intersect each other. From that distance on, the values of r for the 100 mm diameter become lower than those for the 75 mm diameter for the rest of the reactor length. Hence, the outlet values of r are 0.58, 0.60 and 0.61 for the reactor diameters of 50, 100 and 75 mm, respectively. These values show that the conversion efficiency of CH_4 to H_2 and CO is only around 60 %, which means that the residence time in the reactor (roughly 50 – 100 ms for a mean gas axial velocity of 10 – 20 m/s) is too short for the mixture to rich equilibrium. This observation is in agreement with the findings of a previous article [2]. The corresponding values of H_2 and CO mass fractions are given in Table 3. The faster increase of r from 0 to 20 mm axial distance and its higher values for higher diameters from 0 to 350 mm are a result of the faster conversion reactions of reactants (CH_4, O_2) to products (H_2, CO). These are provoked by the larger recirculation zones obtained with higher diameters. The lower values of r from 350 to 1000 mm for the 100 mm diameter reactor than for the 75 mm diameter reactor are explained later, after the discussion on the soot formation. In Figure 8, the axial profiles of the soot mass fraction are given. The picture shows that soot is formed more rapidly and in higher amounts for larger reactor diameters.

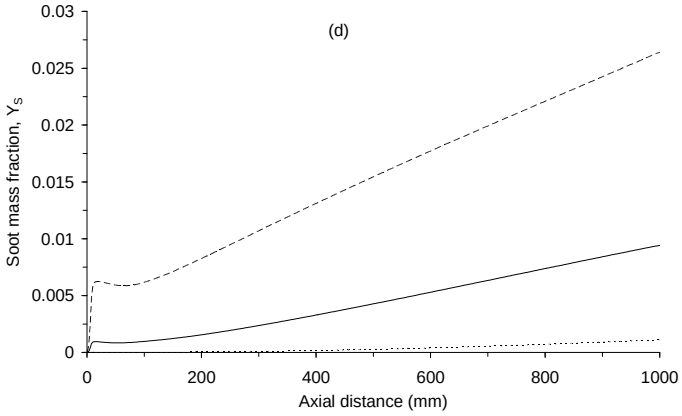

Figure 8 Prediction of axial profiles of the mean of the soot mass fraction for three reactor diameters: 50 mm (dotted line), 75 mm (solid line) and 100 mm (dashed line). The lines have been drawn through the inlet. The results have been

obtained for a premixed NG/NITROX system with equivalence ratio 3.1, pressure 6 bar and initial temperature 673 K.

As found previously, the increase of the reactor diameter leads to faster progress of chemical reactions. This in turn determines the earlier onset of soot formation. In the absence of oxidation, the increase of the soot mass fraction along the reactor is driven by an avalanche process. As a result, the earlier start of soot formation corresponds to higher values of Y_S at the reactor outlet. In this way, the increase of the reactor diameter leads to the increase of the mass fraction of soot. Hence, the mass fraction of soot at the reactor outlet is 0.00125 kg soot/kg for the 50 mm diameter, 0.009 kg soot/kg for the 75 mm diameter and 0.027 kg soot/kg for the 100 mm diameter. The consequences of higher amounts of soot for the larger reactor diameters are the higher heat losses due to radiation and subsequently the lower mixture temperatures. These effects are shown in Figures 9 and 10, where the enthalpy loss variable i and the temperature were plotted, respectively.

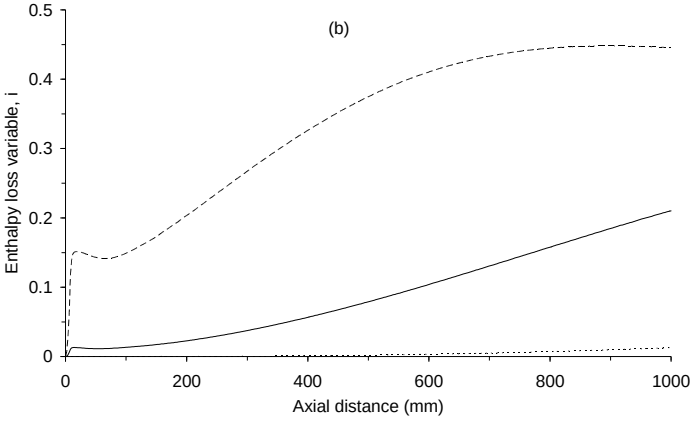

Figure 9 Prediction of axial profiles of the mean of the enthalpy loss variable i for three reactor diameters: 50 mm (dotted line), 75 mm (solid line) and 100 mm (dashed line). The lines have been drawn through the inlet. The results have been obtained for a premixed NG/NITROX system with equivalence ratio 3.1, pressure 6 bar and initial temperature 673 K.

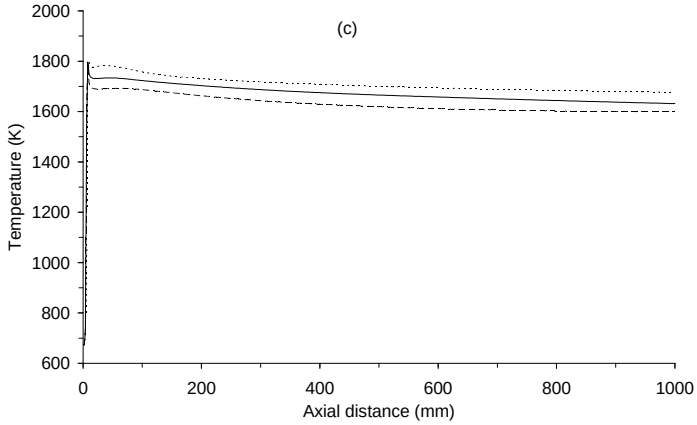

Figure 10 Prediction of axial profiles of the mean of the temperature for three reactor diameters: 50 mm (dotted line), 75 mm (solid line) and 100 mm (dashed line). The lines have been drawn through the inlet. The results have been obtained for a premixed NG/NITROX system with equivalence ratio 3.1.

Summarizing the arguments presented, there are two opposed effects of enlarging the reactor diameter. On one hand, the variable r has a faster initial increase for higher diameters due to better mixing of initial mixture with products. On the other hand, r increases slower along the reactor (smaller slopes of the curves corresponding to larger diameters) because of the raise of the variable i due to heat loss by soot radiation. Higher values of i determine the reduction of the chemical source term of r (lower temperatures). When the latter effect balances the former one, the curves plotted for 75 and 100 mm intersect each other. From that moment on (350 – 1000 mm), the variable r has lower values for 100 mm reactor diameter than for 75 mm reactor diameter, as seen in Figure 7.

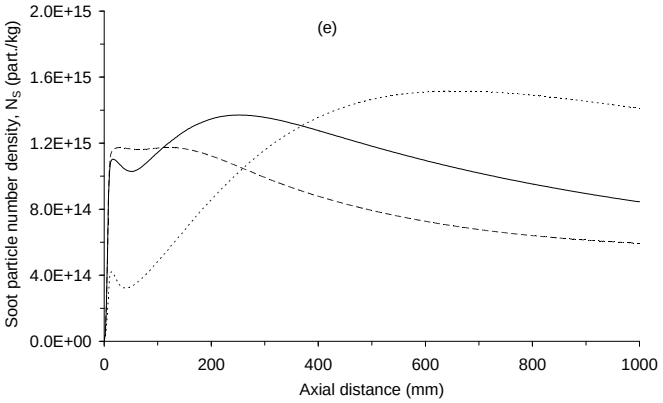

Figure 11 Prediction of axial profiles of the mean of the soot particle number density for three reactor diameters: 50 mm (dotted line), 75 mm (solid line) and 100 mm (dashed line). The lines have been drawn through the inlet. The results have been obtained for a premixed NG/NITROX system with equivalence ratio 3.1, pressure 6 bar and initial temperature 673 K

In Figure 11, the soot particle number density is presented. For all three reactor diameters, the curves show first an increase of the number of particles due to nucleation and then the N_S decreases as a result of soot agglomeration. By correlating the higher number of particles shown in Figure 11 with the lower soot mass fraction revealed in Figure 8 for the lower reactor diameters, we come to the conclusion that the reactors with lower diameter produce less soot with a lower soot mean diameter.

By comparing the simulations results for all three diameters investigated, we can conclude that the reactor with the diameter of 75 mm gives the best conversion of CH_4 to H_2 and CO (highest value of r, H_2 and CO). This reactor shows also a large recirculation zone which insures flame stability and represents a reasonable compromise in view of soot production between the reactor with a diameter of 50 mm, characterized by a very low soot level and the 100 mm diameter reactor which gives a very high soot level.

In Figures 12 and 13 the radial profiles of the reaction progress variable and the soot mass fraction are presented,

respectively. The profiles were depicted for three axial distances measured from the burner tip: x_1 = 5 mm, x_2 = 20 mm and x_3 = 40 mm, as indicated in Figure 3. The case chosen for these plots was the 75 mm diameter reactor. Figure 12 shows that, for the axial distance of 5 mm, r starts with a value of 0.48 in the central recirculation zone, decreases to roughly 0 when intersecting the inlet flow and then increases to 0.41 at the reactor wall. Similar patterns of r are found for the other two axial locations, but the minimum value of r increases with the increase of the axial distance, due to the reduced impact of the inlet flow on the r radial profile. The same observations apply to the soot mass fraction given in Figure 13.

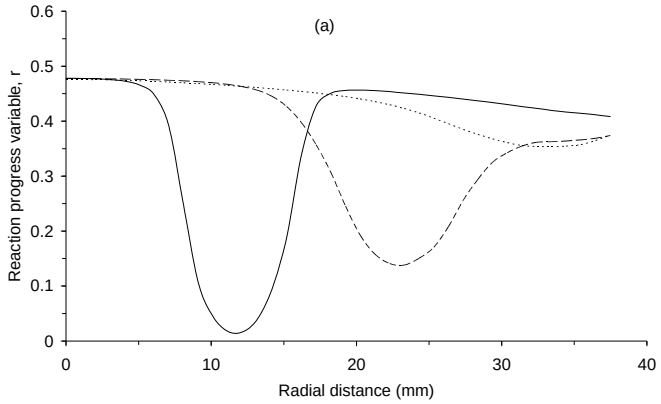

Figure 12. Predictions of radial profiles of reaction progress variable r (a) and soot mass fraction (b) for three axial distances: 5 mm (solid line), 20 mm (dashed line) and 40 mm (dotted line). The results have been obtained for a premixed NG/NITROX system with equivalence ratio 3.1, pressure 6 bar and initial temperature 673 K.

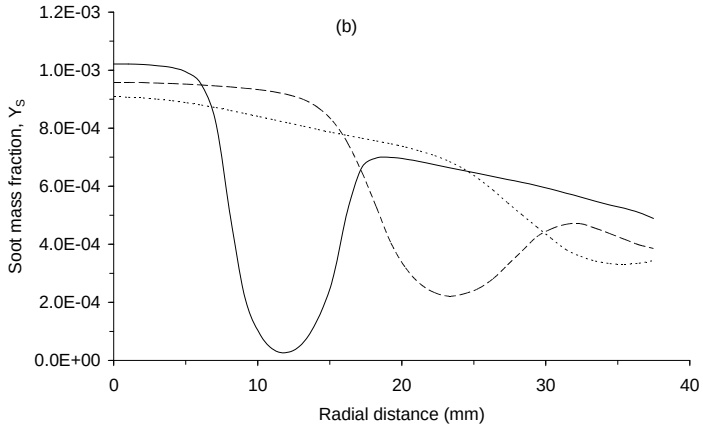

Figure 13. Predictions of radial profiles of soot mass fraction for three axial distances: 5 mm (solid line), 20 mm (dashed line) and 40 mm (dotted line). The results have been obtained for a premixed NG/NITROX system with equivalence ratio 3.1, pressure 6 bar and initial temperature 673 K.

Comparison of measured and predicted product gas composition.

Detailed gas composition measurements were performed in the University of Twente test rig at the nominal point of operation at a natural gas flow equivalent to a power of 300 kW and pressure 3 bar. With the use of the gas chromatograph, off line samples were analysed on concentration of H_2, CO, CO_2 and C_2H_2. The latter species is important as a precursor of soot formation. Table 6 gives the measured concentrations of these species and their values as calculated by the model at 50 ms residence time in the stirred reactor and in the premixed laminar flame and in the equilibrium situation. The important conclusion can be drawn that the measured data for H_2 and CO compare very well with the data in the stirred reactor computation. They are for these species respectively approximately 30%, and 16%. The syngas production as measured in the turbulent reactor and predicted in the stirred reactor is of similar value as predicted in the laminar flame (see table 3 for dry results). Here the rounded H_2 and CO concentrations were 33% and 15% at 50 ms residence time. The equilibrium concentrations are higher by a factor 1.5 as measured for syngas in the turbulent reactor. Hence similar to the PSR calculations, the measured syngas yield,is decreased. An important reason for the decreased yield of syngas is the residual amount of CH_4. In equilibrium all CH_4 is converted to syngas, while both the measurements and the model predictions at 50 ms show a residual CH_4 concentration of 5%. Another explanation for the decreased yield of syngas is the conversion of CH_4 to C_2H_2. This species is absent in equilibrium but both in the measurements and in the model predictions at 50 ms observed at concentrations of 5-7%. Not only this will be at the cost of syngas production, but it will also lead to the formation of soot. The effect of pressure can be assumed to be small, even when increasing the pressure from 1 to 20 bars. The measured operational point at 3 bar compares very well in trend with the other measured points at 1 bar and 50 ms in figure 11. For these reasons a systematic investigation of the effect of pressure was not pursued in the measurements.

Table 3. Comparison of measured and computed exit dry concentrations.

Species concentration [vol %]	H_2	CO	CH_4	CO_2	C_2H_2
Measured in test rig	30.6	16.4	5.0	3.6	7.0
CFD predictions	34.5	18.6	4.9	2.9	2.4
PSR: predicted at 50 ms	29.7	16.0	5.6	3.3	4.5
PREMIX: predicted at 50 ms	32.7	14.9	4.2	3.2	5.4
Chemical equilibrium	44.3	24.1	0	1.5	0

For the University of Twente test rig soot measurements with a SMPS sampling system are scheduled for May 2012. Hence for now a comparison of soot prediction was made for the conditions specified for the premixed flame of reference [16]. This is shown in table 4. It can be remarked that the description of nucleation used here is very crude. It is necessary to use the nucleation constant specified in [16] to obtain good results, instead of the much larger constant specified in [9] !!!!.

Table 4. Predicted soot variables compared to measured by [16].This shows that the model predicts values of soot mass fraction an order of magnitude larger and a particulate number density two orders of magnitude larger. This is in line with the expectations as the flame explored in this paper is very rich, while the flame in [16] is not.

Variable	Present model	Measurements
f_S	4.0E-06	0.3E-06
d_p	2.2E-07	0.25E-07
$N_S \cdot \rho$ (particles/m^3)	7.1E+14 (1.1E+15)	3.0E+16

CONCLUSIONS

The results show that the turbulent rich combustion model is capable of predicting the velocity field, chemical reactions progress, soot formation and heat loss for the partial oxidation of natural gas process. The simulations point out the effect of the reactor diameter and the type of the mixture on the conversion efficiency and the soot production in the partial oxidation process. However, the predictions of soot reported by the model are higher in value than reported for different conditions in the literature. This may be caused by the absence of soot oxidation from the soot formation process, leading to larger predicted values of soot mass fraction. Exoeriemntal validation is expected in the near future.

Based on the simulations of all three diameters investigated, we can conclude that the reactor with the diameter of 75 mm gives the best conversion of CH_4 to products (highest value of r, H_2 and CO). As far as the soot formation is concerned, it represents a reasonable compromise between the reactor with a diameter of 50 mm, characterized by a very low soot level and the 100 mm diameter reactor which gives a very high soot level.

When compared to NG/NITROX mixture, the CH_4/O_2 mixture is characterized by a higher conversion of CH_4 to products, proved by the superior values of the reaction progress variable r, which determines higher mass fractions of H_2 and CO. The back draw is the increased soot formation for the CH_4/O_2 system, resulting in higher soot mass fraction in the mixture. This is accompanied by amplified heat loss to the reactor walls, which lowers the mixture temperature and thus slows down the conversion rate of CH_4 to products.

ACKNOWLEDGEMENTS

The authors would like to thank Dr.Ph Stopfort of ANSYS-CFX for his advice. This research project was supported by the Twente Research School for Process Technology and the Dutch Ministry of Economic Affairs, grant EDI 01015.

REFERENCES

[1] Albrecht, B.A., Kok, J.B.W and van der Meer, Th.H, Co-Production of Syngas and Power by Integration of Partial Oxidation Reactor, Gas Turbine and Air Separation Unit, Int. J. Exergy, vol 4, 357-370, 2007.

[2] Albrecht, B.A., Reactor Modeling and Process Analysis for Partial Oxidation of Natural Gas, PhD thesis, University of Twente, Enschede, 2004.

[3] Geerssen T.M., Physical properties of natural gases, N.V. Nederlandse Gasunie, 1988.

[4] Albrecht, B.A., Kok, J.B.W. and Meer, Th.H. van der, Effect of Pressure, Residence Time, Equivalence Ratio and Type of Oxidizer on Partial Oxidation of Natural Gas, Combust. Sci. and Tech., 181: 1–24, 2009.

[5] Bowman, G., Frenklach, M., Gardiner, B., Smith, G. and Serauskas, B., *GRI-Mech*, Gas Research Institute, Chicago, Ilinois, USA, http://www.me.berkeley.edu/gri-mech/index.html;

[6] CFX-5 flow solver, http://www-waterloo.ansys.com/cfx/products/cfx-5/index.html.

[7] Launder, B. E. and Spalding, D. B., The Numerical Computation of Turbulent Flows, Computer Methods in Applied Mechanics and Engineering, 3, pp. 269-289 (1974).

[8] Brookes, S.J. and Moss, J.B, Predictions of Soot and Thermal Radiation Properties in Confined Turbulent Jet Diffusion Flames, *Combustion and Flame* 116:486 (1999);

[9] Kronenburg, A., Bilger, R.W. and Kent, J.H., Modeling Soot Formation in Turbulent Methane-Air Jet Diffusion Flames, *Combustion and Flame* 121:24 (2000);

[10] Zimberg, M.J. et al., A Study of Coupled Turbulent Mixing, Soot Chemistry, and Radiation Effects Using the Linear Eddy Model, Combustion and Flame 113:454-469 (1998);

[11] Louis, J.J.J., On Turbulent Combustion of Coal Gas, PhD Thesis, University of Twente, Enschede, 1997.

[12] Derksen, M.A.F, On the influence of steam on combustion, PhD thesis University of Twente, Enschede, 2005.

[13] Hu, I.Z. and Correa, S.M., Calculations of Turbulent Flames Using a PSR Microstructural Library, Twenty-Sixth Symposium (International) on Combustion/The Combustion Institute, 1996/pp. 307-313.

[14] Kee, R.J., et al., CHEMKIN Collection, Release 3.6, Reaction Design, Inc., San Diego, CA (2000).

[15] Xu, F., Sunderland, P.B., Faeth, G.M., Soot Formation in Laminar Premixed Ethylene/Air Flames at Atmospheric Pressure, Combustion and Flame 108:471-493 (1997).

[16] Xu, F., Lin, K.C., Faeth, G.M., Soot Formation in Laminar Premixed Methane/Oxygen Flames at Atmospheric Pressure, Combustion and Flame 115:195-209 (1998);

[17] Bockhorn, H., in Soot Formation in Combustion – Mechanisms and Models (H. Bockhorn, Ed.), Springer-Verlag, Berlin Heidelberg New-York, 1994, p. 3;

[18] Bockhorn, H., in Pollutants from Combustion (C. Vovelle, Ed.), Kluwer Academic Publishers, The Netherlands, 2000, pp. 205-239;

[19] Lindstedt, P.R., in Soot Formation in Combustion – Mechanisms and Models (H. Bockhorn, Ed.), Springer-Verlag, Berlin Heidelberg New-York, 1994, p. 417;

[20] Lindstedt, P.R., A Simple Reaction Mechanism for Soot Formation in Non-Premixed Flames, in Proceedings of IUTAM Symposium, Taipei, Taiwan, June 1991 (R.S.L. Lee, J.H. Whitelaw and T.S. Wung, Eds.), Springer-Verlag, Berlin Heidelberg New-York, 1992, p. 145;

[21] Frenklach, M. and Wang, H., in Soot Formation in Combustion – Mechanisms and Models (H. Bockhorn, Ed.), Springer-Verlag, Berlin Heidelberg New-York, 1994, p. 165;

[22] Smoot, L.D., Pratt, D.T., Pulverized-coal combustion and gasification: theory and applications for continuous flow processes, New York, 1979;

[23] Kok, J.B.W., Louis, J.J.J. and Yu, J.H., The IRST Model for Turbulent Premixed Non-adiabatic Methane Flames, *Combust. Sci. and Tech., 1999, Vol. 149, pp. 225-247*.